ORIGINAL RESEARCH

Engineered Exosomes with Growth Differentiation Factor-15 Overexpression Enhance Cardiac Repair After Myocardial Injury

Ailin Zou[1,*], Tingting Xiao[1,*], Boyu Chi[1,2], Yu Wang[1], Lipeng Mao[1,2], Dabei Cai[1,2], Qingqing Gu[1], Qianwen Chen[1], Qingjie Wang[1], Yuan Ji[1], Ling Sun[1,2]

[1]Department of Cardiology, the Affiliated Changzhou Second People's Hospital of Nanjing Medical University, Changzhou, Jiangsu, People's Republic of China; [2]Changzhou Clinical Medical College, Dalian Medical University, Dalian, Liaoning, People's Republic of China

*These authors contributed equally to this work

Correspondence: Ling Sun; Qingjie Wang, Department of Cardiology, the Affiliated Changzhou Second People's Hospital of Nanjing Medical University, Changzhou, Jiangsu, 213003, People's Republic of China, Email sunling85125@hotmail.com; wang-qingjie@hotmail.com

Background: Cardiac repair remains a thorny issue for survivors of acute myocardial infarction (AMI), due to the regenerative inertia of myocardial cells. Cell-free therapies, such as exosome transplantation, have become a potential strategy for myocardial injury. The aim of this study was to investigate the role of engineered exosomes in overexpressing Growth Differentiation Factor-15 (GDF-15) (GDF15-EVs) after myocardial injury, and their molecular mechanisms in cardiac repair.

Methods: H9C2 cells were transfected with GDF-15 lentivirus or negative control. The exosomes secreted from H9C2 cells were collected and identified. The cellular apoptosis and autophagy of H_2O_2-injured H9C2 cells were assessed by Western blotting, TUNEL assay, electron microscopy, CCK-8 and caspase 3/7 assay. A rat model of AMI was constructed by ligating the left anterior descending artery. The anti-apoptotic, pro-angiogenic effects of GDF15-EVs treatment, as well as ensuing functional and histological recovery were evaluated. Then, mRNA sequencing was performed to identify the differentially expressed mRNAs after GDF15-EVs treatment.

Results: GDF15-EVs inhibited apoptosis and promoted autophagy in H_2O_2 injured H9C2 cells. GDF15-EVs effectively decreased the infarct area and enhanced the cardiac function in rats with AMI. Moreover, GDF15-EVs hindered inflammatory cell infiltration, inhibited cell apoptosis, and promoted cardiac angiogenesis in rats with AMI. RNA sequence showed that telomerase reverse transcriptase (TERT) mRNA was upregulated in GDF15-EVs-treated H9C2 cells. AMPK signaling was activated after GDF15-EVs. Silencing TERT impaired the protective effects of GDF15-EVs on H_2O_2-injured H9C2 cells.

Conclusion: GDF15-EVs could fulfil their protective effects against myocardial injury by upregulating the expression of TERT and activating the AMPK signaling pathway. GDF15-EVs might be exploited to design new therapies for AMI.

Keywords: exosomes, growth differentiation factor-15, telomerase reverse transcriptase, acute myocardial infarction

Introduction

Acute myocardial infarction (AMI) remains a culprit of death worldwide. Early prevention, effective intervention and appropriate care have reduced the mortality of AMI, but survivors may still face the risk of lethal complications, due to post-infarction scar formation, pathological remodeling, and ventricular arrhythmias.[1,2] Therefore, post-infarction myocardial repair has slipped into the research hotspot, especially that about cell therapy.[3] For example, cardiomyocyte and stem cell transplantation have been advocated, but transplanted cells manifest a poor survival and a low plasticity, both of which lead to unsatisfactory outcomes.[4,5] In contrast, recent research advances have demonstrated that paracrine bioactive molecules from cardiomyocytes can activate endogenous tissue repair and regeneration.[6,7] Collective evidence supports that cardiomyocyte-derived exosome transplantation can improve cardiac function after MI, with advantages of easy exosome isolation and expansion, mild immune rejection, and a high success rate.[8,9] In this cell-free therapeutic strategy,

bioactive molecules are transferred directly into injured recipient cells to reduce pathological inflammation, inhibit cardiomyocyte apoptosis, necrosis and remodeling, as well as promote neovascularization.[3,10]

Autocrine and paracrine communication between cells regulates tissue or organismal function. To provide specific signaling and targeted delivery, cells secrete membrane vesicles and distribute them into the peripheral blood, urine, saliva and other body fluids. Extracellular vesicles can be categorized based on diameter size, as mentioned in MISEV guidelines (2018). Usually, EVs < 100 nm or <200 nm in diameter are considered as small or medium, and those >200 nm as large EVs. In contrast, exosomes are a subclass of extracellular vesicles 40–150 nm in diameter.[11] Packed by plasma membrane-derived lipid bilayers, they harbor various bioactive molecules, such as lipids, proteins, and RNAs that are involved in an array of biological processes.[12] The performance of exosomes in intercellular communication has been actively investigated.[6,13] Exosomes generated from a mixture of cardiomyocytes, endothelial and smooth muscle cells can promote cardiac regeneration, with benefits equivalent to those of injections of human induced pluripotent stem cells, but do not increase the risk of complications, such as arrhythmias, tumorigenicity, as well as immune rejection.[14,15]

Growth differentiation factor-15 (GDF-15), a protein from the transforming growth factor superfamily, governs various biological processes, such as inhibiting inflammatory response, apoptosis and cell growth.[16] Recent studies have found that GDF-15 helps to protect from cardiovascular diseases.[17,18] Under a physiological condition, GDF-15 is barely expressed in tissues, but its expression increases significantly in cardiomyocytes damaged by ischemia and stress, thus making it a biochemical marker for cardiovascular diseases. Plasma GDF-15 concentration associates with the prognosis of AMI and the choice of therapeutic regimen, and independently predict the risk of adverse cardiovascular events.[19,20] Recent studies have plucked out an association between GDF-15, inflammation and cardiac fibrosis during heart failure and infarction, and GDF-15 may protect against cardiovascular diseases by modulating the metabolic activity and repressing oxidation, inflammation, apoptosis, and fibrosis in H9C2 cells.[21,22]

Here, we investigated how transplantation of H9C2 cells-derived exosomes with GDF-15 overexpression regulates cellular apoptosis and autophagy to benefit cardiac repair in a post-infarction left ventricular remodeling model.

Methods
Cell Culture and H_2O_2 Exposure
Commercial rat H9C2 cells (BOSTER, CX0111) were purchased and cultured in Dulbecco's modified Eagle medium (DMEM, Gibco, USA) supplemented with 10% fetal bovine serum (FBS, Gibco, USA), 100 U/mL penicillin, 100 μg/mL streptomycin and 110 mg/mL sodium pyruvate. All cells were incubated at 37°C in a humidified atmosphere containing 5% CO_2, and the fluid was changed once every 1–2 days. When the cell density reached 80%–90%, 1:3 passages were made; P3, P4 generation cells were used. H9C2 cells were exposed to a serum-free medium containing 200 μM H_2O_2 for 12 hours. The H_2O_2 concentration and treatment time were determined by CCK-8 and Caspase-3/7 assays in pre-experiments. The exposed cells were simultaneously treated with PBS, GDF15-EVs or NC-EVs, respectively.

Lentiviral Transduction
Lentivirus overexpressing GDF-15 and control virus were purchased from GENECHEM. Before transfection, the medium was changed to low-serum medium with 1% FBS. The titers of these two viruses were 1×10^8 TU/mL, ie, 1×10^8 biologically active virus particles per milliliter of virus solution. MOI (Multiplicity of Infection) is the ability of a virus to infect a cell; a higher MOI indicates a weaker ability. The ratio of the number of viral particles used to infect 80% of the cells to the number of cells is usually regarded as the MOI of the cell. MOI = viral titer (TU/mL) × viral volume (mL)/number of cells. Pre-transfection was performed with MOI values of 1, 10 and 100, respectively. At 72 hours after virus addition, fluorescence intensity was observed by fluorescence microscopy, and the optimal MOI of 100 was finally determined to ensure a maximum transfection efficiency. After formal transfection, the virus was transfected for 24 hours. The medium containing the virus was carefully withdrawn and replaced with normal medium, and then put back into the incubator for culture. The fluorescence from GFP was observed under Zeiss fluorescence inverted microscope after 72 hours. The transfection results were verified by Western blotting (WB). After confirming the fluorescence intensity of lentivirus in the cells, the cells were seeded into T25 culture flasks, and screened with 0.75 ug/mL of puromycin for 72 hours. Afterward, the medium was replaced, and the cells

continued to be cultured in the incubator. The H9C2 cells with stable overexpression of GDF-15 (GDF-15^{OE}-CMs) and the controls (GDF- 15^{NC}-CMs) were prepared.

Exosome Isolation and Characterization

Rat H9C2 cells were cultured to 70% confluence in complete DMEM; then the complete medium was replaced with DMEM supplemented with 10% exosome-free FBS. Exosome-free FBS was prepared by centrifuging FBS at 120,000g for 18 hours, and passing it through a 0.22-μm filter (Millipore, SLGP033RB). Forty-eight hours later, the culture medium was collected, centrifuged at 2000 g for 30 minutes and at 10,000 g for 30 minutes, passed through a 0.22-μm filter to remove the cellular debris, and then centrifuged at 120,000 g for 70 min. The supernatant was removed, and the pellet was resuspended in phosphate-buffered saline (PBS); then, the mixture was centrifuged again at 120,000g for 70 min, and the pellet, which contained already-isolated exosomes, was resuspended in 100 μL PBS and stored at −80°C. Transmission electron microscopy (TEM) and Nanoparticle Tracking Analysis (NTA) were used to determine particle morphology and particle size distribution of isolated exosomes. According to the NTA report, the total concentrations of GDF15-EVs and NC-EVs were 1.6×10^{10} Particles/mL and 8×10^{9} Particles/mL in 100 μL PBS, respectively. We then calculated the numbers of two exosomes per mL of medium as 2×10^{9} and 1×10^{9}, respectively. The expression levels of exosome markers CD63, CD81 and TSG101 were detected by WB.

Exosome Uptake Assessments

Dil (red fluorescent dye, Beyotime, C1991S) was diluted to a concentration of 5 mmol/L with DMSO solution and stored at −20°C. Briefly, every 50 μg (1 μg/μL) of exosomes were added to 1 μL of Dil and incubated for 15 minutes in the dark. To remove excess dye, 3 mL of PBS and Exosome Isolation Reagent were mixed and centrifuged at 1500×g for 30 minutes. Supernatant was then aspirated, and the Dil-labeled exosomes were resuspended in 50 μL of PBS. H9C2 cells were seeded onto a 96-well plate until a confluence of 60%, and then co-cultured with Dil-labeled EVs for two time periods (6 hours, 24 hours). Then, the cells were washed with PBS and fixed with 4% paraformaldehyde for 20 min. The nuclei were stained with 6-diamino-2-phenylindole (DAPI, Beyotime, C1005) for 10 min and subsequently visualized using a fluorescence microscope.

CCK-8 Assay

Cell viability was determined using Cell Counting Kit-8 (CCK-8, Yeasen, 40203ES76) assay. The cells were counted and then seeded into 96-well plates. After an 8-hour culture, the medium reached a confluence of 50%. Then, different volumes of exosomes (10 μg, in 10 μL of PBS) or 10 μL of PBS were added into the wells. After a 24-hour incubation, the culture medium was discarded, and 10μL of CCK-8 solution was added to each well and incubated at 37°C for 2 hours, the absorbance was analyzed at 450 nm using a Microplate Reader.

TUNEL Assay

Terminal deoxynucleotidyl transferase-mediated dUTP nick end labeling (TUNEL) (Ribobio, China) was applied to detect cell apoptosis. Briefly, the cells were cultured in 96-well plates in the medium until a confluence of 60%. Then, the culture medium was discarded, and 10 μL of GDF15-EVs (1 μg/uL), 10 uL of NC-EVs (1 μg/uL) or 10 μL of PBS were added. The cells in each treated group were immobilized with 4% paraformaldehyde at room temperature, washed twice with PBS and incubated with buffer containing 0.1% Triton X-100 on ice for 10 min, and finally washed and sealed with 3% BSA. The slides were further incubated with 50 μL of freshly prepared TUNEL reaction mixture for 1 h at 37°C in a humidified chamber. Fluorescent images were acquired with fluorescence microscopy (AE31, Motic, Xiamen, China).

Caspase-3/7 Assay

Caspase-3/7 assays were used for cell apoptosis. Caspase-3/7 apoptosis detection kit (RiboBio, R11094.2) was used to detect apoptosis. The cells were cultured in 96-well plates in the medium. After an 8-hour culture, the medium reached a confluence of 60%. Then, different volumes of exosomes (10 μg, in 10 μL of PBS) or 10 μL of PBS were added into the wells. After a 24-hour incubation, the culture medium was discarded, and the cell nucleus were stained with Hoechst

33,342. Early apoptotic cells were stained with caspase-3/7. PI staining was used for late apoptosis. The apoptosis rate was calculated for subsequent analysis.

Western Blotting Assay

Total protein was extracted from myocardial tissues, and its concentration quantified with a bicinchoninic acid (BCA) kit. The protein was separated by 10% sodium dodecyl sulfate–polyacrylamide gel electrophoresis (SDS–PAGE) and then transferred to polyvinylidene fluoride (PVDF) membranes, using a semidry transfer system (Bio–Rad, USA). The membrane was blocked in 5% defatted milk powder for 2 h at 37°C, washed with phosphate buffer solution with Tween 20 (PBST), incubated with primary antibodies against Bcl-2, Bax, P62, Lc3, TERT, AMPK, P-AMPK and GDF-15 overnight at 4°C, then washed with PBST (5 times × 3 min), then with of horseradish peroxidase (HRP)-labeled secondary antibodies for 1 h 30 min at 37°C. Enhanced chemiluminescence (ECL) was used for visualization. ImageJ was used for gray value analysis. With GAPDH or β-Actin as a loading control, the relative expression of target proteins was measured as the gray value ratio of target protein to that of GAPDH or β-Actin.

Quantitative Real-time-polymerase Chain Reaction (qRT-PCR)

Total RNA and mRNA were extracted from exosomes, cells and tissues with Trizol reagent (Vazyme, R401-01). The cDNA libraries of mRNA were synthesized using HiScript II 1st-Strand cDNA Synthesis kit (Vazyme, R211-01). Quantitative real-time PCR (RT-qPCR) was accomplished with HiScript II One step qRT-PCR SYBR Green kit (Vazyme, Q221-01). The level of mRNA was normalized to that of GAPDH, and the data were calculated via comparative $2^{-\Delta\Delta Ct}$. Each experiment was triplicated and repeated at least three times independently. The primer sequences used are as follows: GAPDH-f-5′-AGAACATCATCCCTGCCTCTACT-3′, GAPDH-r-5′-GATGTCATCATATTTGGCAGGTT-3′; TERT-f-5′-GCAGAAGAC AGTGGTGAACTT-3′, TERT-r-5′-CTTAATTGAGGTCCGTCCGTAAC-3′.

AMI Models and Exosome Injection

Rats were randomized into different groups. SD rats (weight 200–220g) were anesthetized by intraperitoneal injection of pentobarbital sodium (50 mg/kg) before the surgical procedure. A 6–0 polyester suture was used to ligate the left anterior descending coronary artery (LAD). Exosomes were injected into the border zone of the infarcted hearts at 30 minutes after ligation, as previously described.[23] Briefly, every 100 μL of exosomes (1 μg/μL) or 100 μL of PBS was injected into the border zone of the infarcted hearts at three locations.

Echocardiography

wo and four weeks after surgery, transthoracic echocardiography was performed to evaluate cardiac function. Echocardiography was performed as previously described,[13] using a Vevo2100 digital imaging system (Visual Sonics) in rats under 1% isoflurane. M mode measurements were acquired in the parasternal short-axis view at the level of the papillary muscle. Left ventricular ejection fraction (LVEF), left ventricular fractional shortening (LVFS), left ventricular diameter (LVD), left ventricular anterior wall (LVAW), left ventricular posterior wall (LVPW) and left ventricular weight (LVW) were measured and calculated during the analysis. Calculation of the LVW values was carried out using the following formula: $LVM = 1.05 \times \left[(LVDd + LVPWd + LVAWd)^3 - LVDd^3 \right]$. The left ventricular ejection fraction (EF) was calculated by the cubic method: $LVEF\ (\%) = \left((LVIDd)^3 - (LVIDs)^3 \right)/(LVIDd)^3 \times 100\%$, and the left ventricular fractional shortening (FS) was calculated by $LVFS\ (\%) = (LVIDd - LVIDs)/LVIDd \times 100\%$. The data from four cardiac cycles were averaged.[24]

Histological Analysis

Rats were sacrificed after echocardiography measurements were recorded. Then, the tibial length of the rats was measured. Masson's trichrome and Sirius red staining were implemented to quantify the extent of infarction and fibrosis in the left ventricle (LV) with ImageJ software. Hematoxylin–eosin (HE) staining was used to roughly evaluate the degree of inflammatory infiltration. Vascular density was quantified by immunofluorescence of CD31. Apoptotic cells

were counted by TUNEL assay. Immunohistochemical staining was used to evaluate the positive rate of BCL-2, NLRP3, and Cleaved Caspase-3.

Enzyme-Linked Immunosorbent Assay (ELISA)

Three days following myocardial injury, peripheral blood samples (500 μL) were collected from rats. Plasma was separated from ethylenediaminetetraacetic acid (EDTA) anti-coagulated blood samples of rats by centrifugation at 1000 rpm/min for 15 minutes. The plasma was then separated and stored at −80°C until further analysis. The concentrations of IL-6 (Cat No. PI328), TNF-α (Cat No. PT516) and IL-10 (Cat No. PI525) were detected using the enzyme-linked immunosorbent assay (ELISA) kit according to the manufacturer's instructions (Beyotime, China).

mRNA Sequencing and Bioinformatic Analyses

mRNA sequencing was performed in both GDF15-EVs and NC-EVs treated H9C2 cells. mRNA sequence was analyzed by RiboBio (Guangzhou, China) using the Illumina HiSeq^{TM} 2500 instrument. Differentially expressed mRNA were identified by |log 2(FoldChange)|> 1 and P value <0.05. Bioinformatic analyses were performed, including differential expression mRNA analysis, mRNA target gene prediction, GO analysis, and KEGG pathway enrichment analysis.

Transfection Experiment

si-TERT mRNA (50 nmol/L) (Supplementary Table 1) and negative control mRNA (50–100 nmol/L) synthesized by Guangzhou Ribobio were transfected into H9C2 cells using riboFECT™ CP Reagent (C11062-1, Ribobio, China). qRT-PCR was performed to determine transfection efficiency. At 48 hours after transfection, different groups of cells were harvested for subsequent experiments.

Statistical Analysis

All data were expressed as mean ± standard error of mean (SEM) and subjected to GraphPad Prism 8 (GraphPad Software, San Diego, CA, USA). Comparisons between two groups were assessed by the Student t test. One-way ANOVA was used to compare three or four groups. $P < 0.05$ was considered as statistical significance.

Results

GDF-15 Overexpression Reduced Apoptosis and Promoted Autophagy of H9C2 Cells

H9C2 cells were transfected with lentivirus-GDF-15 (Figure 1A) and empty lentivirus vectors. The green fluorescence of GDF-15^{OE}-CMs and GDF-15^{NC}-CMs verified successful lentiviral transfection (Figure 1B). WB revealed that GDF-15^{OE}-CMs elevated the expression of GDF-15 protein, compared with GDF-15^{NC}-CMs (Figure 1C and D). Subsequently, TUNEL assay showed that GDF-15^{OE}-CMs significantly reduced cell apoptosis, compared to the GDF-15^{NC}-CMs (Figure 1E and F). CCK-8 assay observed that cell viability significantly increased after GDF-15 overexpression (Figure 1G). WB suggested that apoptosis marker Bax and autophagy marker P62 expression fell, and apoptosis marker Bcl-2 and autophagy marker Lc3 expression rose in the GDF-15 overexpression group (Figure 1H–K). Overall, GDF-15 overexpression significantly reduced apoptosis and promoted autophagy of H9C2 cells.

Isolation and Identification of GDF15-EVs

Exosomes were isolated from GDF-15^{OE}-CMs and GDF-15^{NC}-CMs. Exosomes in a cup-shaped morphology could be observed in both groups (Figure 2A). Three specific markers of exosomes, TSG101, CD81 and CD63 were positive in both groups (Figure 2B). To identify whether these exosomes were endocytosed by H9C2 cells, we incubated H9C2 cells with exosomes labeled with Dil for different durations. After 6 hours and 24 hours of incubation, red signals were detected in the H9C2 cells. Confocal images confirmed the uptake of labeled exosomes in a time-dependent manner. GDF15-EVs were more effectively taken up by H9C2 cells after a 24-hour incubation
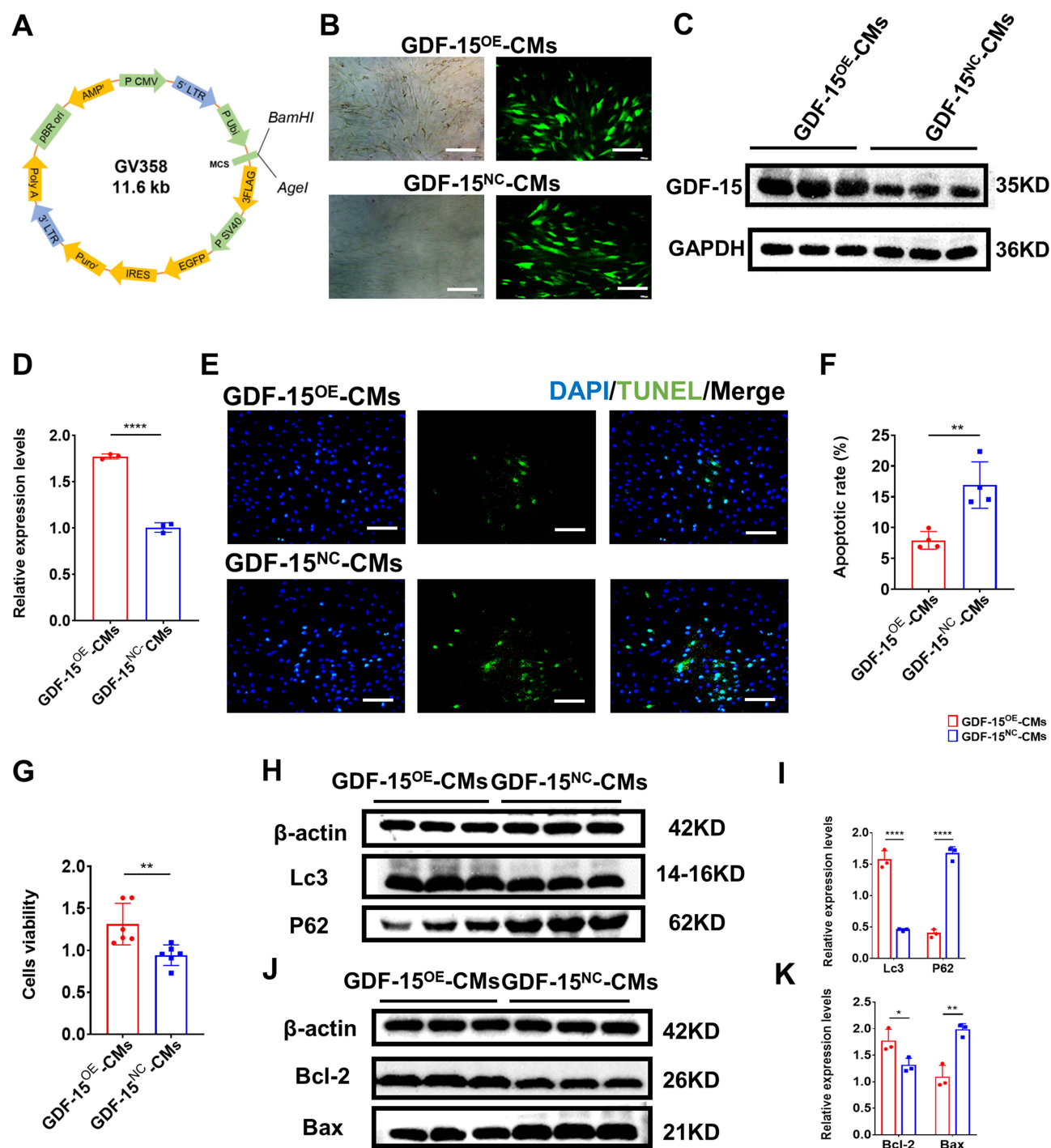
Figure 1 GDF-15 overexpression reduced apoptosis and promoted autophagy in cardiomyocytes. (**A**) Diagram of the GV358 after insertion of GDF-15 gene. (**B**) Successful lentiviral transduction was confirmed by positive fluorescence signal under a microscope in both GDF-15^{OE}-CMs and GDF-15^{NC}-CMs groups (Scale bar =200 μm). (**C**) WB images showed GDF-15 protein levels in GDF-15^{OE}-CMs and GDF-15^{NC}-CMs groups; (**D**) quantification analysis (n=3). (**E**) Cell apoptosis was analyzed by TUNEL assay and (**F**) quantification analysis (n=4) (Scale bar =200 μm). (**G**) Cell viability was analyzed by CCK8 assay (n=6). (**H**) WB of the autophagy markers in different groups; (**I**) quantification analysis (n=3). (**J**) WB of apoptosis markers in different groups; (**K**) quantification analysis (n=3). *P < 0.05, **P < 0.01, ****P < 0.0001.

(Figure 2C). NTA showed that the size and concentration distribution of exosomes were similar between GDF15-EVs and NC-EVs group (Figure 2D and E). GDF-15 protein level was significantly higher in exosomes secreted by H9C2 cells with GDF-15 overexpression than that in NC-EVs (Figure 2F and G).
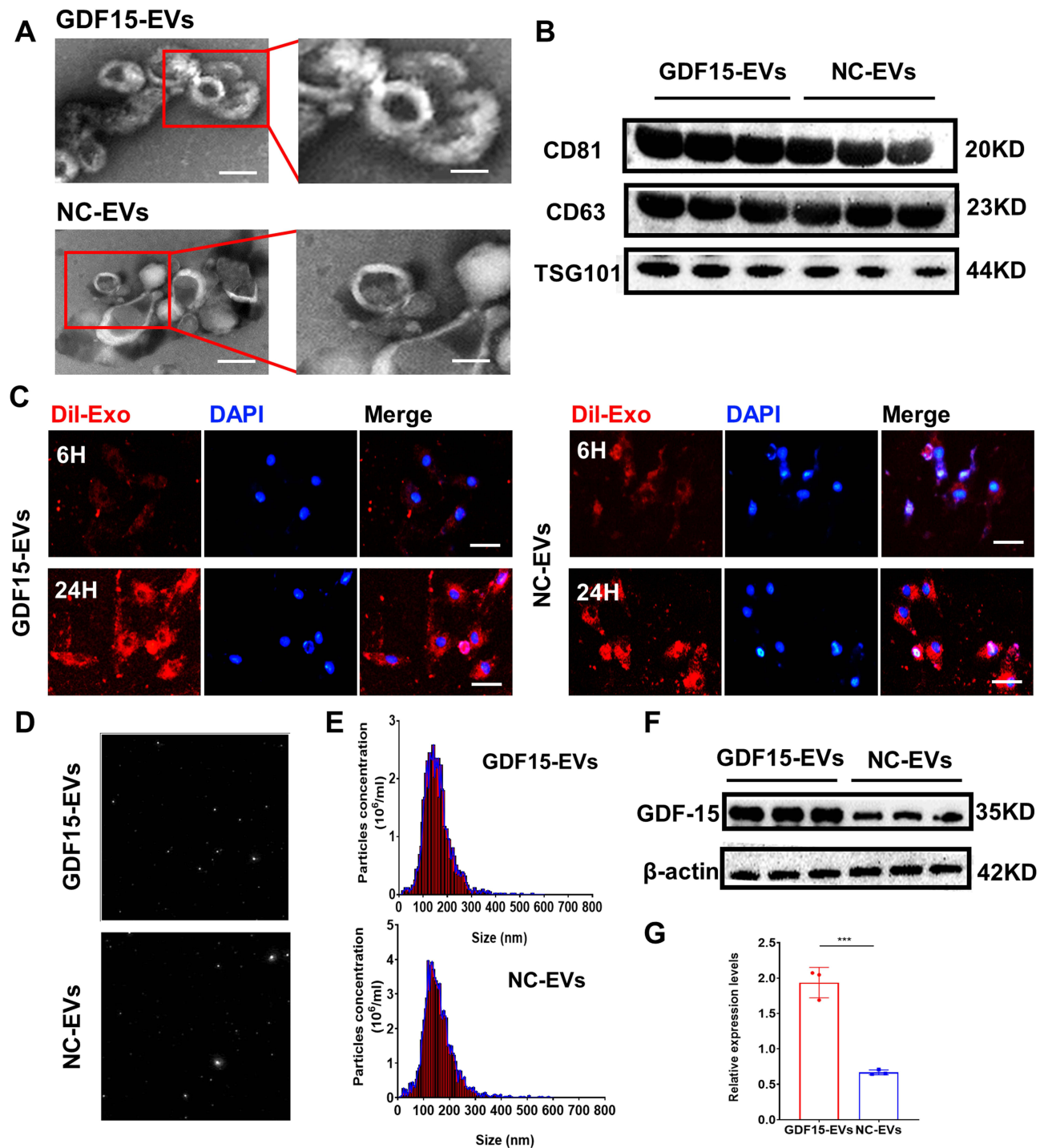
Figure 2 Isolation and identification of exosomes from cardiomyocytes. (**A**) TEM images of exosomes isolated from GDF-15^{OE}-CM and GDF-15^{NC}-CM groups (n=3) (right: scale bar =50 nm, left: scale bar =100 nm). (**B**) WB for TSG101, CD63 and CD81 in exosomes (n=3). (**C**) Confocal images showed that the red fluorescence of dye Dil labeled exosomes from two groups cells was endocytosed by H9C2 at 6 and 24 h after incubation. Scale bar=50 μm (n=3). (**D** and **E**) NTA for size and concentration of exosomes isolated from H9C2 cells (n=3). (**F**) WB images showed GDF-15 protein levels in GDF15-EVs and NC-EVs groups; (**G**) quantification analysis (n=3). ***p<0.001.

GDF15-EVs Reduced Apoptosis and Promoted Autophagy in H$_2$O$_2$-Injured H9C2 Cells

We further evaluate the protective effects of GDF15-EVs in vitro. Firstly, TUNEL assay showed that the GDF15-EVs significantly reduced cell apoptosis induced by H$_2$O$_2$, compared to that in the NC-EVs group (Figure 3A and B). CCK-8 assay observed that cell viability was significantly increased after GDF15-EVs treatment (Figure 3C). Transmission electron
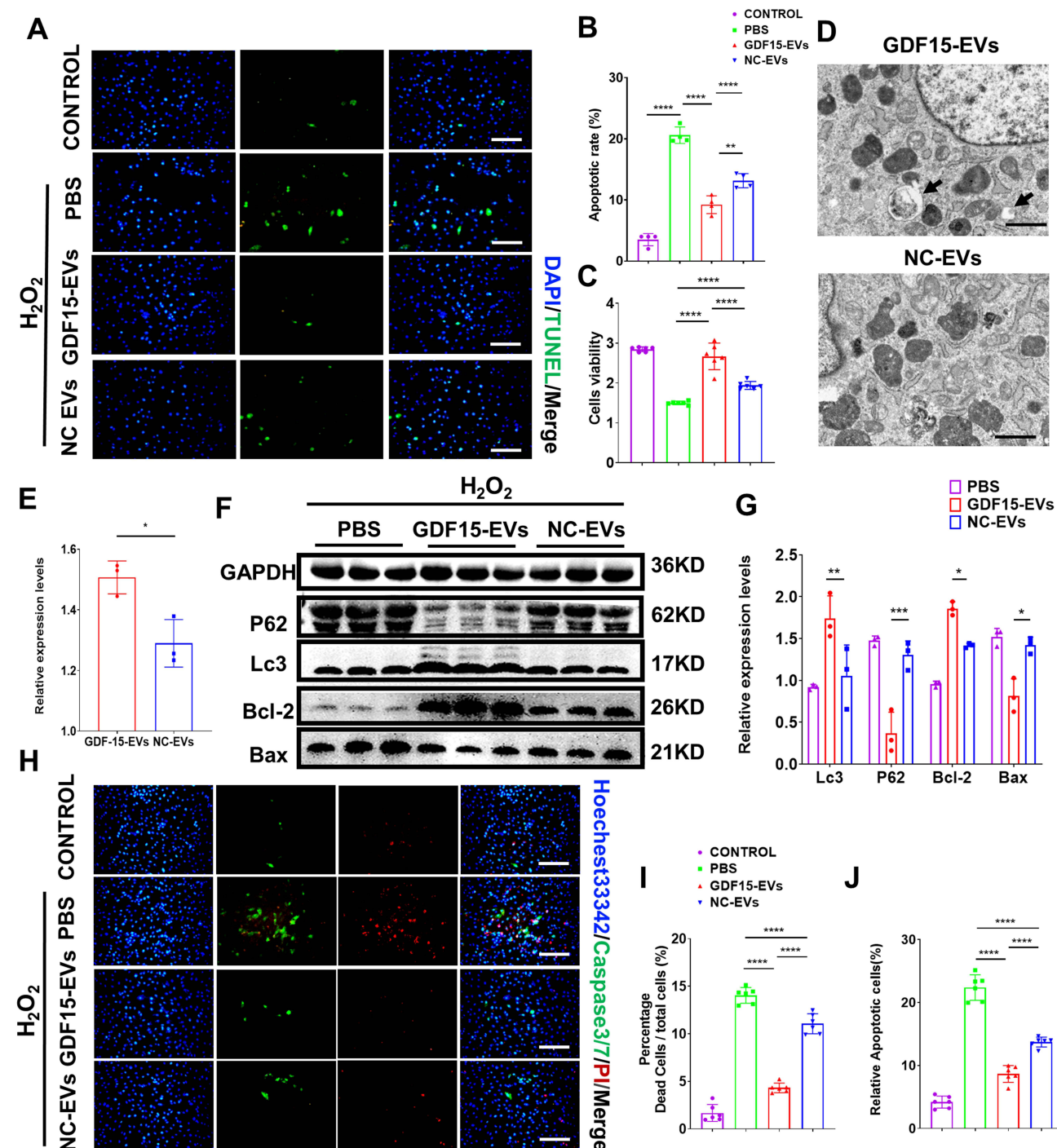
Figure 3 GDF15-EVs reduced apoptosis and promoted autophagy in H_2O_2-injured cardiomyocytes in vitro. (**A**) Cell apoptosis was analyzed by TUNEL assay; (**B**) quantification analysis (n=4 for each group) (Scale bar =200 μm). (**C**) Cell viability was analyzed by CCK8 assay (n=6). (**D**) The autophagy in H9C2 cells was observed with TEM; the black arrows represented the autophagosomal structures; (**E**) quantification analysis. (Scale bar =20 μm). (**F**) WB of autophagy and apoptosis markers in different groups; (**G**) quantification analysis (n=3). (**H**) Hoechest33342/PI/Caspase3/7 staining was used to observe the survival of H9C2 cells treated with normoxic condition, H_2O_2, GDF15-EVs and NC-EVs after H_2O_2-induced injury. Quantitative analysis of (**I**) viable cells and (**J**) caspase 3/caspase 7 positive cells between the four groups. (Scale bar =200 μm). *P < 0.05, **P < 0.01, ***P<0.001, ****P < 0.0001.

microscopy revealed that autophagosome structures, characterized by a double-membrane structure containing cargo, increased in GDF15-EVs-treated H9C2 cells (Figure 3D and E). This finding suggested that exosomes from GDF-15^{OE}-CMs induced autophagy in H_2O_2-injured H9C2 cells. Moreover, WB suggested that apoptosis marker Bax and autophagy maker P62 expression fell, and apoptosis marker Bcl-2 and autophagy marker Lc3 expression rose in the GDF15-EVs group (Figure 3F and G). GDF15-EVs and NC-EVs weakened caspase3 and caspase7 activity and prevented apoptosis in H9C2 cells

under H_2O_2 injury (Figure 3H–J). At the same time, these effects were more evident in the GDF15-EVs group. Our results showed exosomes derived from GDF-15^{OE}-CMs reduced apoptosis and increased autophagy and viability of H9C2 cells.

GDF15-EVs Decreased Infarct Area and Enhanced Cardiac Function in Rats with AMI

To evaluate the cardioprotective effects of exosomal treatments, GDF15-EVs, NC-EVs or PBS (AMI control group) were injected into the infarct zone border of rat hearts within 30 minutes after AMI. Masson's trichrome staining exhibited smaller infarct and fibrotic areas at 28 days in the GDF15-EVs group than in the PBS and NC-EVs groups (Figure 4A and B). Figure 4C and D show echocardiographic images of rats' hearts in each group at 14 and 28 days after myocardial infarction, respectively. The left ventricular ejection fraction (LVEF) and left ventricular fractional shortening (LVFS) were calculated from the images to evaluate left ventricular systolic function. Echocardiography performed at 14 days after MI showed a significantly improved LVEF in the GDF15-EVs group (57.08% ± 0.77%), compared to the AMI (25.34% ± 2.51%, P < 0.01) and NC-EVs groups (39.75% ± 2.34%, P < 0.05) (Figure 4E). In addition, LVFS was significantly higher in the GDF15-EVs group (30.98% ± 0.33%), compared to those in all the other groups (AMI: 12.75% ± 0.99%, P < 0.01 vs NC-EVs: 20.79% ± 1.18%, P < 0.05) (Figure 4F). At 28 days after MI, the GDF15-EVs group (51.34% ± 2.21%) also showed a significant increase in LVEF, compared to the AMI (24.27% ± 2.86%, P < 0.01) and NC-EVs groups (39.03% ± 0.82%, P < 0.05) (Figure 4G). Echocardiographic data further indicated that the rats injected with GDF15-EVs had a higher LVFS than those injected with PBS (27.14% ± 1.37% vs 11.53% ± 1.92%, P < 0.01) and NC-EVs (19.75% ± 0.59%, P < 0.05) (Figure 4H). Therefore, at 14 and 28 days after infarction, the LVEF and LVFS of rats in the GDF15-EVs group were significantly higher than those in the AMI and NC-EVs groups, indicating preserved systolic function in the former group of rats. To further elucidate the effects of GDF15-EVs on post-infarction myocardial remodeling, left ventricular weight (LVW) and tibial length were measured. At 28 days after infarction, GDF15-EVs significantly reduced the LVW to tibial length ratio (LVW/TIBIA) to attenuate pathological myocardial hypertrophy in rats, compared to those in the NC-EVs or AMI group (Supplementary Figure 1). The remaining echocardiographic parameters of the LV for four groups are shown in Supplementary Tables 2 and 3. These findings demonstrated that GDF15-EVs could effectively inhibit myocardial fibrosis, preserve cardiac function, and reduce ventricular remodeling, compared to the other groups after myocardial infarction.

GDF15-EVs Repressed Inflammatory Infiltration, Cell Apoptosis, and Enhanced Angiogenesis in Rats with AMI

Inflammation and subsequent fibrosis are typical pathological events in scar formation after MI. Therefore, we used H&E staining to assess the degree of inflammation in the infarcted heart. We observed a significantly decrease in inflammatory cell infiltration in the GDF15-EVs group, compared with the AMI group (Figure 5A). Regarding the early inflammatory response, the serum levels of IL-6, TNF-α and IL-10 were quantified by enzyme linked immunosorbent assay (ELISA) assay on the 3rd day after exosome injection. The results showed that GDF15-EVs significantly reduced IL-6 and TNF-α concentrations and obviously increased IL-10 concentration, compared with those in AMI and NC-EVs groups (Figure 5B–D). Immunohistochemical results showed that GDF15-EVs or NC-EVs treatment reduced the expression of the proinflammatory factor NLRP3 at 28 days after myocardial infarction. Furthermore, GDF15-EVs exhibited superior anti-inflammatory properties compared with NC-EVs (Supplementary Figure 2A and B). Overall, these results demonstrated that GDF15-EVs could effectively attenuate post-MI inflammation. We then used Sirius red staining to assess the post-MI fibrotic area in each group. Sirius red staining at 4 weeks after MI showed a reduction in collagen area in the GDF15-EVs group (Figure 5E and F). Immunohistochemistry results showed a higher deposition of brownish-yellow granules in the cytoplasm of the GDF15-EVs group (Figure 5G). Image analysis confirmed that the average optical density (AOD) of BCL-2 in the GDF15-EVs group (0.1357± 0.011) was increased compared with that in the AMI group (0.0697 ± 0.0250, p < 0.001) or NC-EVs group (0.0953 ± 0.0463, P < 0.05) (Figure 5H). This indicated that GDF15-EVs treatment exhibited a strong anti-apoptotic ability after infarction. To further reveal the mechanism of this exosomal treatment, immunofluorescence with antibodies against CD31 and TUNEL was used to display capillary density and cell apoptosis. Four weeks after AMI, the capillary density in the myocardial boarder zone significantly increased in the GDF15-EVs group compared with those in PBS and NC groups (Figure 6A and B). TUNEL results
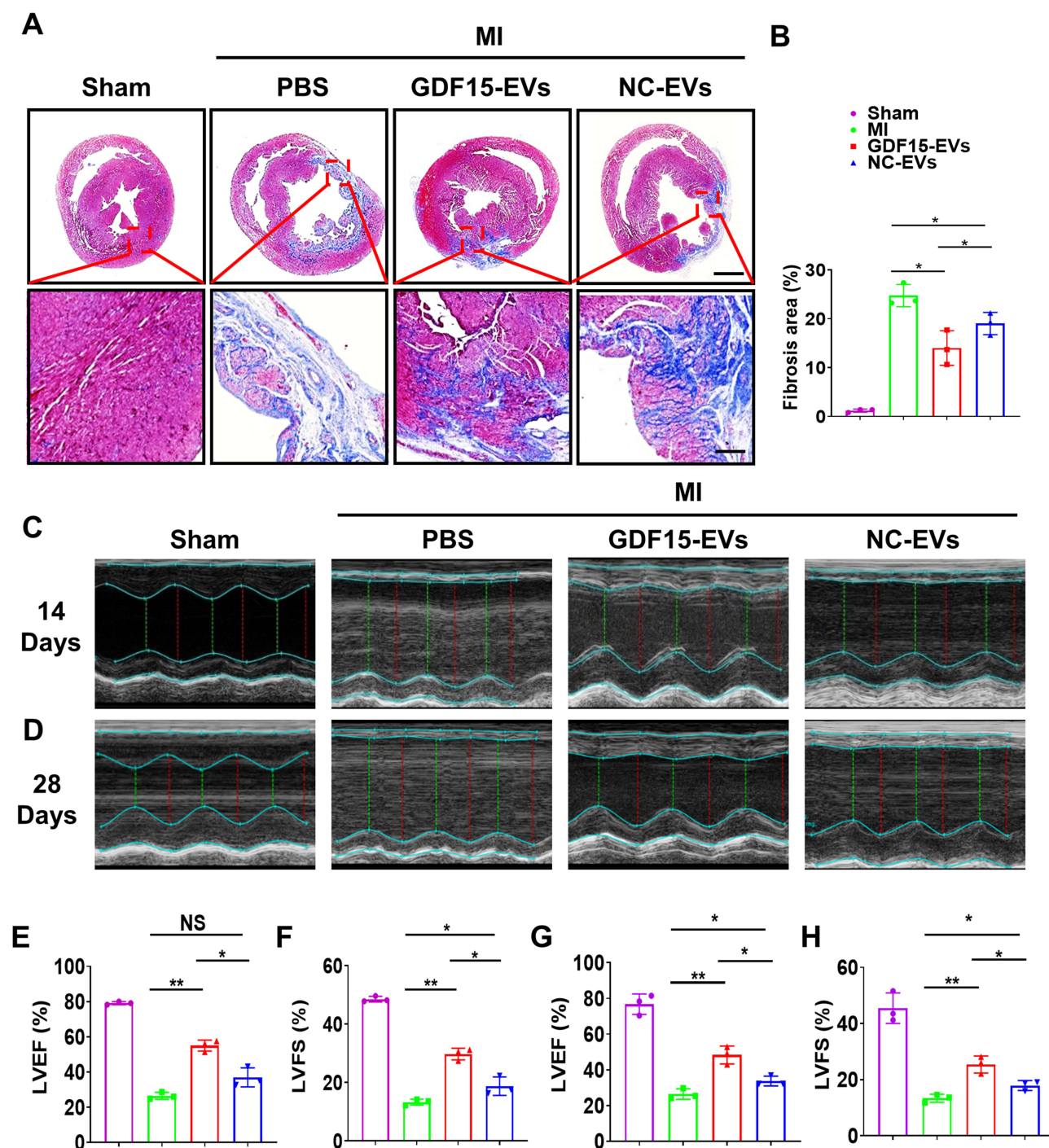
Figure 4 Intramyocardial injection of GDF15-EVs reduced infarct size and improved cardiac function after AMI. (**A**) Masson's trichrome staining was performed to estimate the degree of myocardial fibrosis at 4 weeks post-AMI; (**B**) quantitative analysis for the fibrotic area (n=3) (Scale bar =1000 μm, 200 μm). (**C**) Representative images of echocardiograms of rat hearts at 14 days post-AMI. (**D**) Representative images of echocardiograms of rat hearts at 28 days post-AMI. Quantitative analysis of (**E**) LVEF and (**F**) LVFS (n=3 for each group) at 14 days post-AMI. Quantitative analysis of (**G**) LVEF and (**H**) LVFS (n=3 for each group) at 28 days post-AMI. *P < 0.05, **P < 0.01.

showed that the GDF15-EVs group exhibited significantly fewer apoptosis and TUNEL positive rate (Figure 6C and D). Furthermore, the expression of Cleaved Caspase-3 was analyzed using immunohistochemistry. After 28 days of MI, immunohistochemical detection revealed a significant decline in the protein expression of Cleaved Caspase-3 in the GDF15-EVs group (Supplementary Figure 2C and D). The above results suggested that GDF15-EVs exerted their effects on myocardial repair by enhancing angiogenesis and improving cell survival.
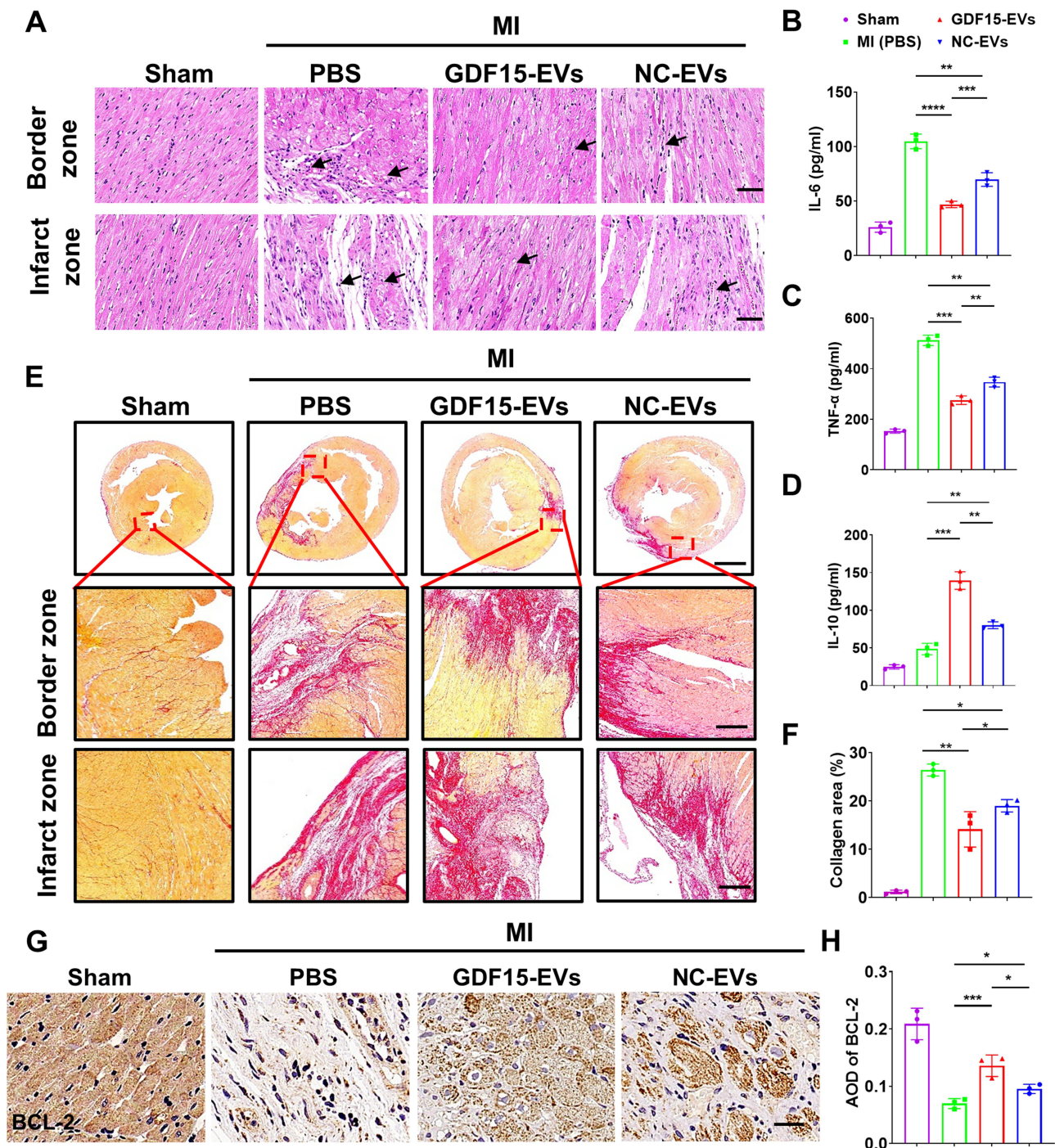
Figure 5 Intramyocardial injection of GDF15-EVs inhibited fibrosis and reduced inflammation in infarcted hearts (**A**) H&E staining at the border zone and infarct zone at 28 days after MI (scale bar =200 μm). The black arrows indicated the degree of inflammatory cell infiltration in the infarct 28 days post-infarction. (**B–D**) ELISA analysis of IL-6, TNF-α and IL-10 concentrations in serum of MI induced rats after treated by PBS, GDF15-EVs or NC-EVs (n = 3). (**E**) Representative images of Sirius red staining; (**F**) quantification of the collagen area (n=3) (Scale bar =1000 μm, 200 μm). (**G**) Representative images of immunohistochemistry analysis for BCL2 expression in different groups and (**H**) quantification analysis of AOD (n=3) (Scale bar =20 μm). Data are shown as the mean ±SEM. *P < 0.05, **P < 0.01, ***p<0.001, ****p<0.0001.

Differentially Expressed mRNA in H9C2 Cells After GDF-15 EVs Treatment

In order to explore the molecular mechanisms involved in the cardioprotective effects of GDF15-EVs, mRNAs sequencing was performed on GDF15-EVs and NC-EVs treated H9C2 cells. The heatmap indicated that 63 mRNAs were up-regulated and 50 were down-regulated in GDF15-EVs, compared with those in NC-EVs treated H9C2 cells.
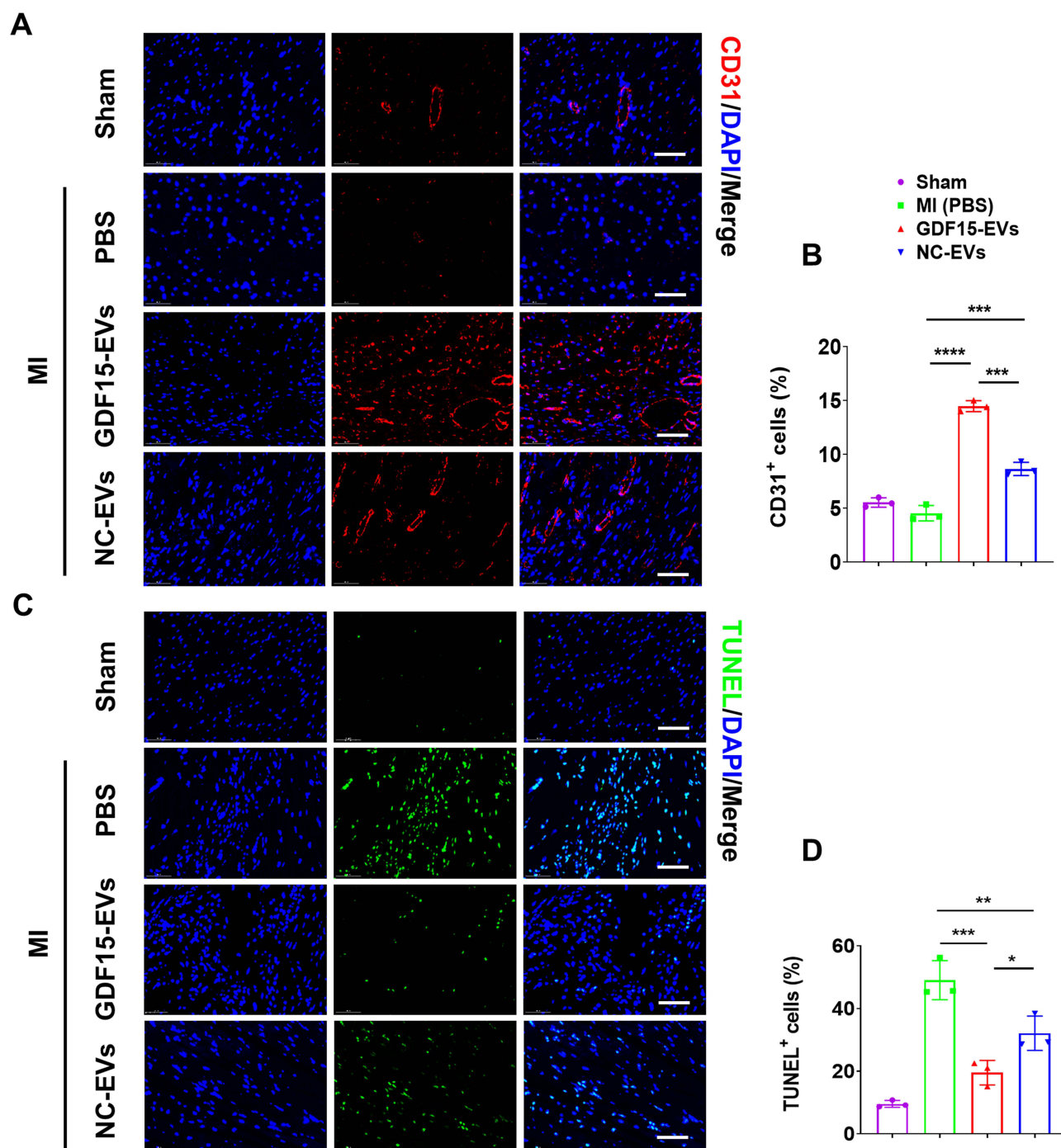
Figure 6 GDF15-EVs promoted angiogenesis and reduced apoptosis in a rat AMI model in vivo. (**A**) Representative images of CD31 positively stained capillaries; (**B**) quantification analysis (n=3) (Scale bar = 200 μm) (**C**) Representative images of TUNEL staining at the border zone; (**D**) quantification analysis. (n=3) (Scale bar = 200 μm). Data are shown as the mean ±SEM. *P < 0.05, **P < 0.01, ***p<0.001, ****p<0.0001.

TERT (Telomerase Reverse Transcriptase) presented the highest mRNA level, which has been demonstrated to inhibit apoptosis and promote autophagy in many diseases (Figure 7A–C). Further, these mRNAs were submitted to GO enrichment analysis. The enriched terms in molecular function, cellular component, and biological process of these mRNAs are shown in Figure 7D.[25] It has been demonstrated that in TERT-deficient mice, telomeres are significantly shortened, which results in upregulation of P53 and downregulation of Ki67, both associated with increased apoptosis, decreased proliferation and cellular hypertrophy in cardiomyocytes, and ultimately left ventricular enlargement, ventricular wall thinning, and impaired cardiac function.[26–28]
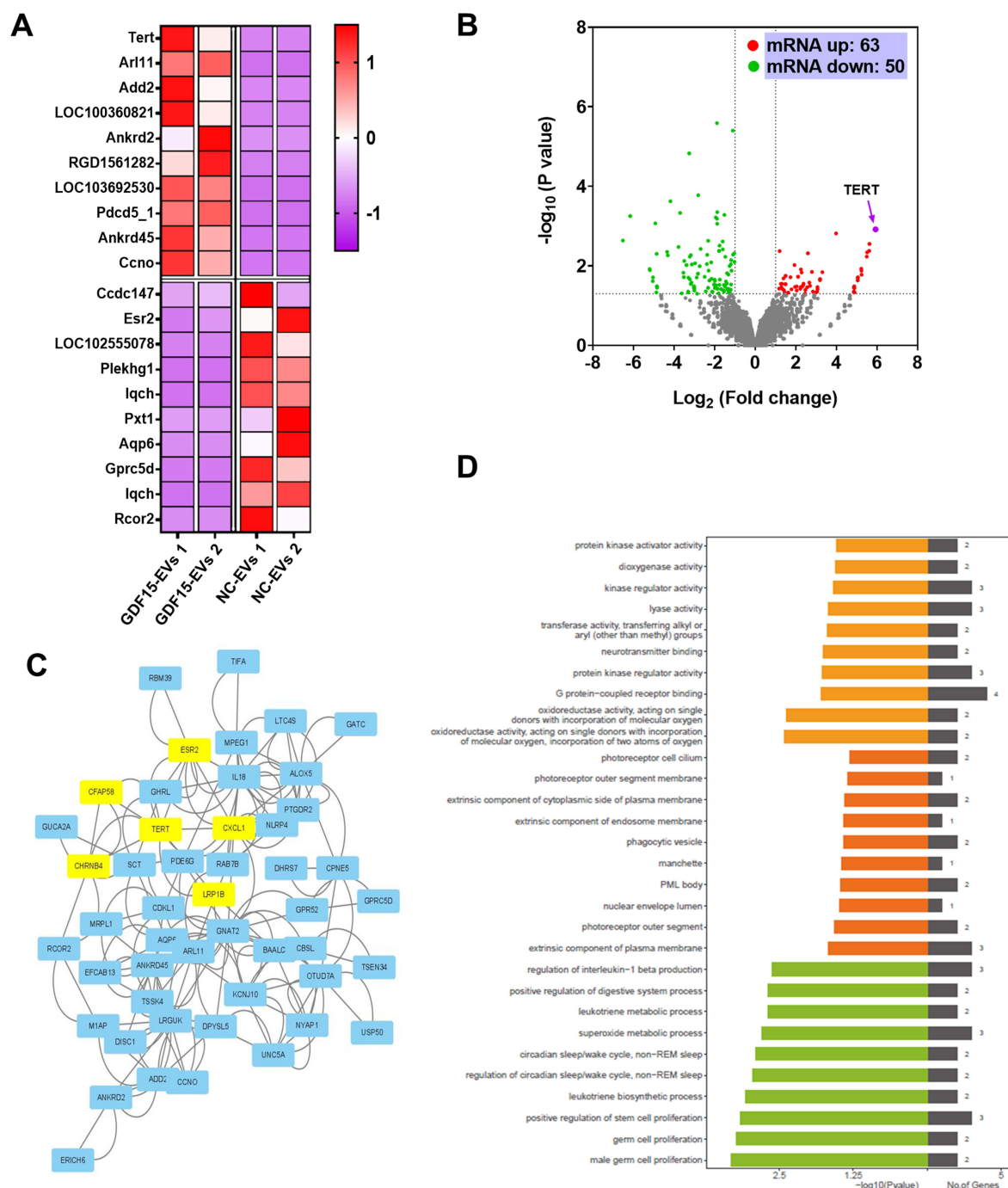
Figure 7 Differentially expressed mRNAs between GDF15-EVs and NC-EVs treated cardiomyocytes. (**A**) Heatmap of upregulated and downregulated mRNAs (red represents high expression and purple represents low expression) between GDF15-EVs and NC-EVs group. (**B**) Volcano plot showing the significantly differentially expressed mRNAs (2-fold change and p<0.05 as the threshold) between GDF15-EVs and NC-EVs groups. (**C**) The overlap of upregulated mRNAs in GDF15-EVs group according to mRNA sequencing analysis. (**D**) GO enrichments of mRNAs in molecular function, cellular component, biological process.

Silencing TERT Impaired the Protective Effects of GDF15-EVs on H₂O₂-Injured H9C2 Cells

Next, whether TERT mediates the cardioprotective effect of GDF15-EVs was further verified. GDF15-EVs and NC-EVs were added to H₂O₂-injured H9C2 cells, respectively. We then tested the protein levels of TERT in H9C2 cells treated with GDF15-EVs and NC-EVs. GDF15-EVs significantly increased the protein level of TERT in H₂O₂-injured H9C2 cells, compared to that in the NC group (Figure 8A and B). To further identify the signaling pathways responsible for the
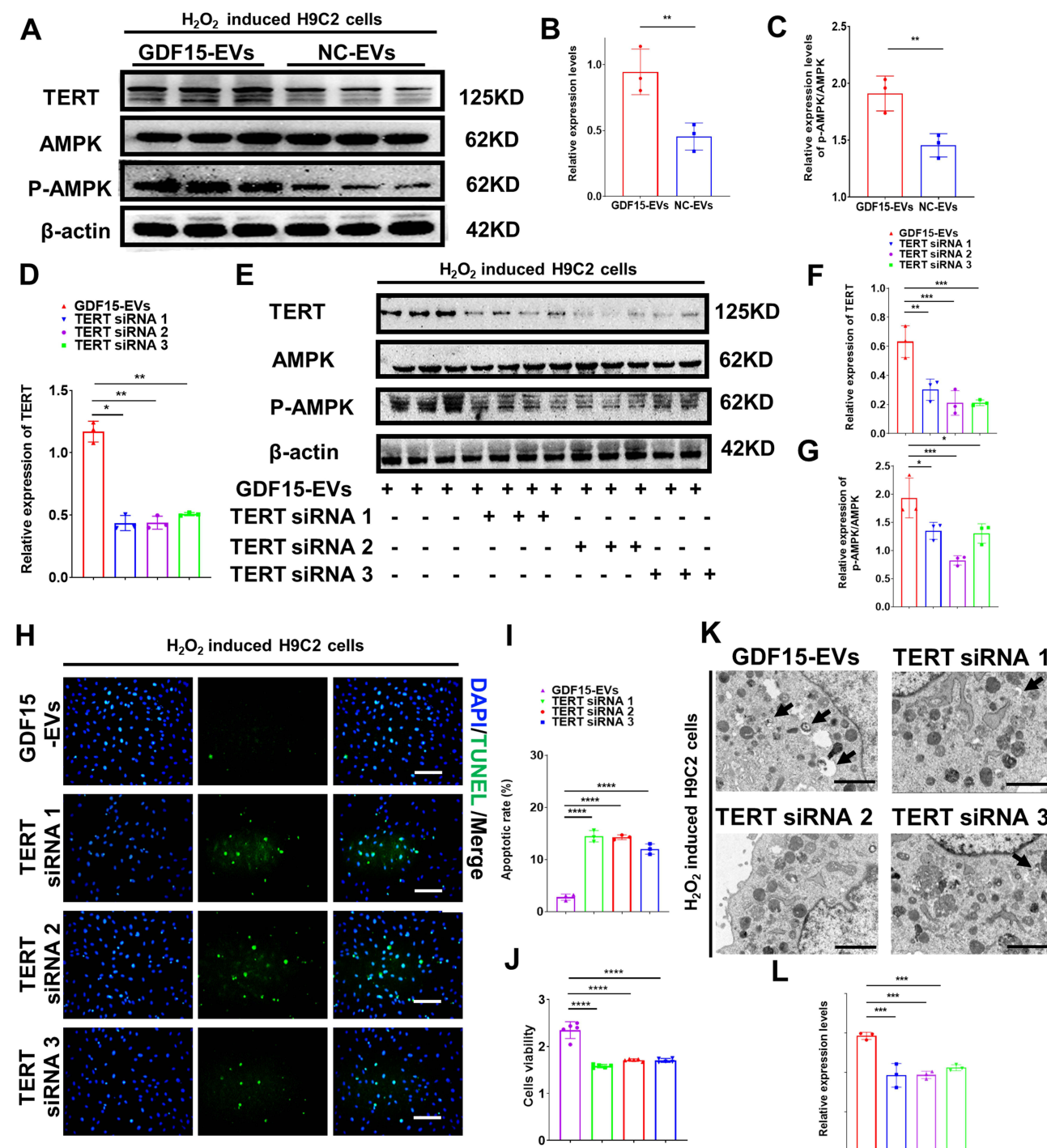
Figure 8 Silencing TERT impaired the protective effects of GDF15-EVs in H_2O_2-injured cardiomyocytes. (**A**) WB of TERT protein, AMPK and P-AMPK protein in GDF15-EVs and NC-EVs treated groups and (**B** and **C**) quantification analysis (n=3). (**D**) qRT-PCR validation of TERT mRNA levels in GDF15-EVs treated group and cardiomyocytes transfected with si-TERT (n=3). (**E**) WB of TERT, AMPK and p-AMPK protein in cells under different treatments and (**F** and **G**) quantification analysis (n=3). (**H**) Cell apoptosis was analyzed by TUNEL assay in GDF15-EVs and siRNA groups and (**I**) quantification analysis (n=3). (Scale bar = 200 μm). (**J**) Cell viability was analyzed by CCK8 assay (n=6). (**K**) The autophagy in H9C2 cells was observed with TEM and (**L**) quantification analysis. The black arrows point to autophagosomal structures. (Scale bar = 20 μm). *P < 0.05, **P < 0.01, ***p<0.001, ****P < 0.0001.

effect of GDF15-EVs, we incubated H9C2 cells with GDF15-EVs and NC-EVs under H_2O_2. We found enhancement of AMPK protein phosphorylation, which is an important link in cell autophagy (Figure 8C).[29,30]

To confirm the essential role of TERT in the cardioprotective function of GDF15-EVs, we performed a loss-of-function study of TERT in H9C2 cells under H_2O_2. H9C2 cells were transfected with TERT siRNA, and their function was quantified by qRT-
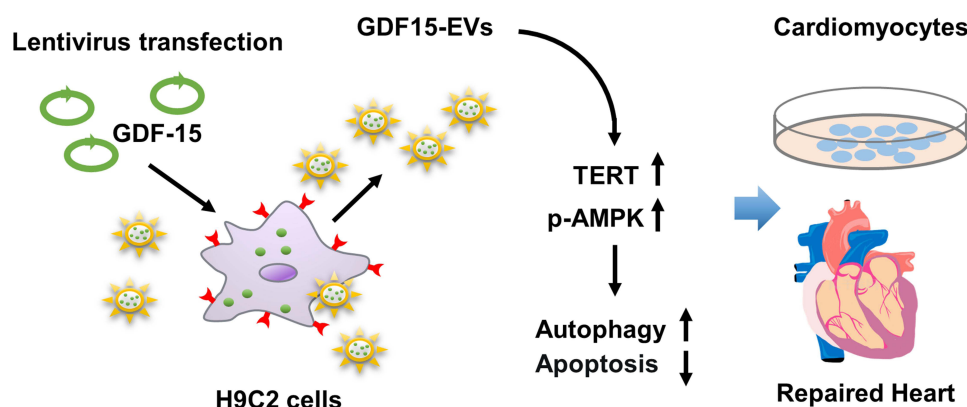
Figure 9 Schematic showed the working model of this study. EVs released by cardiomyocytes with GDF-15 overexpression inhibited apoptosis and promote autophagy of H_2O_2-injured cardiomyocytes via enhanced expression of TERT mRNA.

PCR. After transfection, TERT mRNA level in H9C2 cells was significantly lower than that in the GDF15-EVs treatment group (Figure 8D). WB also verified the same result at the protein level, and we observed a lower level of AMPK phosphorylation after cotransfection with siRNA, suggesting that the AMPK pathway was suppressed in the GDF15-EVs treatment group (Figure 8E– G). In addition, TUNEL assay suggested that silencing TERT expression reversed the antiapoptotic effect of GDF15-EVs, as evidenced by a significant increase in dead cells (Figure 8H and I). Meanwhile, CCK8 assay demonstrated that the increase in cell viability after GDF15-EVs treatment was attenuated by cotransfection with TERT siRNA (Figure 8J). Furthermore, the electronic microscopy reported a decreased expression of autophagosomes in the siRNA group, compared to that in the GDF15-EVs group (Figure 8K and L). Thus, silencing TERT blocked the effect of GDF15-EVs in promoting autophagy after injury. Taken together, all our experimental results suggest that the exosomes secreted from the GDF-15[OE]-CMs might upregulate the expression of TERT to activate the AMPK pathway, thus promoting the repair in H_2O_2-injured H9C2 cells (Figure 9).

Discussion

AMI can subject cardiomyocytes to apoptosis and necrosis, resulting in irreversible damage to the myocardium. Although some cardiomyocytes may survive, the heart has lost its capability of supplying sufficient blood across the whole body.[31,32] Given the non-renewable characteristics of the myocardium, myocardial repair remains a challenge. Cardiomyocytes transplantation has been trialed, but few cells survive, even followed by intense immune responses. Exosomes are considered as new candidate therapies that play an important role in intercellular and tissue-level communication in stem cell therapy for acute myocardial infarction while overcoming some of the limitations of stem cell therapy.[24,33,34]

In recent years, more and more studies have been conducted on exosomes and their potential therapeutic applications. Many publications have demonstrated that exosomes can attenuate injury in animal models of AMI and in cell culture models. Literature data have emphasized that stem cell-derived exosomes can improve AMI in preclinical models.[35] Therefore, exosome-based therapy has been proposed as a novel therapeutic option in CVDs. The pre-clinical studies conducted to date are concerned with the usage of exosome-like vesicles for drug delivery to treat several potential diseases, such as different types of cancers, cardiovascular diseases, Parkinson's and Alzheimer's disease.[36] EVs have been used in clinical studies to target drug delivery of cancer therapies but never applied to the field of cardioprotection.[37] Many researchers, including our team, are investigating the effectiveness of exosomes in animal models of acute myocardial infarction. Studies have shown that exosomes are involved in many cardiovascular physiological and pathological processes. These studies could then address many of the issues in preclinical exosome therapy (ie, determination of the cellular source, route of administration, exosome dosage, duration of treatment, and post-infarction follow-up).

Numerous studies have demonstrated that cardioprotective effects of cardiomyocytes rely on the transfer of exosome-packaged bioactive proteins, RNAs, and lipids.[38,39] Exosomes have retained the biological activity of their origin cells,

but also demonstrate higher immune tolerance and proliferation stability, thus offering them safety and reproducibility in clinical use.[40,41] GDF-15, a stress protein, has been extensively studied in recent years as a cardioprotective factor.[42] Under normal conditions, GDF-15 hide their beneficial effects; but under stressful conditions, GDF-15 is increasingly secreted to repair the myocardium.[43,44] Then, we speculated that the paracrine secretion of GDF-15 from H9C2 cells might be boosted for myocardial repair.

In the present study, in vitro experiments demonstrated that exosomes with GDF-15 overexpression exerted a protective effect against myocardial infarction, by enhancing cell autophagy and viability and inhibiting apoptosis under H_2O_2. In vivo experiments further confirmed that GDF15-EVs improved cardiac function in a post-infarction rat model, by reducing fibrosis size and inflammatory response, promoting angiogenesis, and inhibiting myocardial apoptosis. In this study, we utilized targeted delivery of GDF15 by extracellular vesicles and evaluated its feasibility and efficacy for the treatment of ischemic heart disease. In addition, mRNA sequencing showed upregulation of TERT mRNA, suggesting its importance in the cardioprotective effects of GDF15-EVs. Recent studies have found that TERT can be expressed in nonproliferative or low-proliferative tissues, such as the heart and vascular system. Cardiomyocyte apoptosis was significantly reduced in transgenic mice overexpressing TERT. Moreover, by specifically targeting the TERT overexpression vector in cardiomyocytes, the area of myocardial infarction could be reduced and the survival rate of mice could be improved, which are evidences that TERT has a protective effect in the cardiovascular system. Finally, we demonstrated that delivery of GDF15 through extracellular vesicles upregulated TERT mRNA to activate the AMPK signaling pathway, thereby promoting cardiac repair in H9C2 cells.

Myocardial ischemia often causes myocardial hypertrophy, fibrosis, inflammation, and persistent stiffness.[45] Telomeres are located at the ends of eukaryotic chromosomes and help maintain their integrity.[46,47] Telomerase contains telomerase reverse transcriptase (TERT) and its RNA component (TERC).[48] As cells divide, telomeres shorten progressively till to their function loss and genomic instability, resulting in cellular senescence or apoptosis, such as that in cardiovascular disease.[25,49] Telomere abnormalities can decrease myocardial contractility, upregulate pro-apoptotic transcription factors, facilitate cellular hypertrophy and senescence.[50] Studies have shown that TERT in mitochondria improves mitochondrial function to reduce cell death in the damaged region after myocardial injury, thus promoting the recovery of cardiac function.[51–53] It has also been found that the HIF-1α/TERT axis can induce autophagy through the mTOR pathway under hypoxic stress conditions.[54,55] There is growing evidence that autophagic dysfunction plays a key role in myocardial ischemic injury. Previous studies provided limited insights into the effects of the cardioprotective ability of GDF15 acting on downstream proteins, which prompted us to use sequencing in our study to investigate the effects of downstream proteins after GDF15-EVs treatment. The results showed that TERT was significantly upregulated. Therefore, in the present study, we wanted to further validate the specific mechanism by which TERT exerts its ability to promote myocardial repair in H9C2 cells treated with GDF-15 overexpressing exosomes.

As with the downstream mechanism of TERT mRNA in GDF-15 EVs treatment H9C2 cells, we further uncovered that TERT could activate the AMPK signaling pathway, which is known to be widely involved in cell autophagy and apoptosis. This downstream mechanism implies that GDF15-EVs can play a role in myocardial repair by inhibiting apoptosis as well as enhancing autophagy. At the same time, our study found that the protective effect of GDF15-EVs against H_2O_2-induced myocardial injury was significantly attenuated after TERT mRNA silencing, supporting that GDF15-EVs enable myocardial repair by upregulating TERT mRNA and stimulating the AMPK signaling pathway. This method provides new insight into the clinical translation of exosome-based therapy for AMI.

Stem cell therapy for myocardial infarction has attracted unprecedent attention over decades. Bone marrow mesenchymal stem cells (BMSCs) have been introduced into myocardial infarction transplantation therapy, due to their unique properties, such as easy accessibility, multidirectional differentiation potential and absence of immune response. Nevertheless, in the ischemic cardiac microenvironment, the cardiac cells have a poor survival, thus limiting the therapeutic efficacy of bone marrow mesenchymal stem cells, as well as prompting the exploration for mechanisms of exosomes in cardiac repair and new and effective approaches.[56] Exosomes, extracellular vesicles secreted by a variety of cells, act as an important carrier for the crosstalk between cells. Compared with cell-based transplantation therapy, exosomal treatment, as an emerging cell-free therapy, has the advantages of low immunogenicity, biodegradability, high tolerance, high stability and non-toxicity.[57,58]

Our previous studies have shown that exosomes derived from mesenchymal stem cells can protect myocardium from heart injury.[59] Recent studies have described the miRNA profiles in exosomes derived from of human induced pluripotent stem cells (iPSCs) and their differentiated cardiomyocytes (iPSCs-CMs).[60] They have found that the exosomes secreted by iPSCs-CMs have different characteristics. For example, miR-1-3p, which is essential for cardiac development and pathology, is only found in the exosomes from iPSC-CMs. The exosomes from iPSCs-CMs are also rich in miR-133a-3p, miR-208b-3p and other molecules that have been clarified to have protective effects on cardiac function. It has also been confirmed in another study that exosomes from iPSCs-CMs can promote cardiac repair after AMI in the swine.[61] Therefore, we speculated that exosomes produced by H9C2 cells may play specific roles in cardiac repair. Our current study confirmed that exosomes from GDF15 engineered H9C2 cells could exert cardioprotective effects by inhibiting the apoptosis and promoting the autophagy of cardiac cells. In future studies, iPSCs-CMs may be selected as mother cells for exosomes used for designing autologous and allogenic therapies.

Nevertheless, there are still several limitations in this study. First, the sustainability of exosome treatment was not verified, and the duration of myocardial protection by GDF15-EVs could be prolonged by some bioengineering methods in the subsequent experiments. Second, whether the cardioprotective effects by TERT will cause tumor and inflammatory tendency in other organ sites and whether there are some unpredictable toxic side effects need to be explored in the next experiments.[47] Finally, the cardioprotective effects of GDF15-EVs need to be further verified by large-size animal experiments and clinic studies. In addition, the safety of GDF15-EVs treatments should be trialed before administration in patients with heart injury.

Conclusion

GDF15-EVs protect against myocardial injury by upregulating the expression of TERT and activating the AMPK signaling pathway. GDF15-EVs could be employed to design a promising therapy for AMI.

Abbreviations

AMI, acute myocardial infarction; GDF15-EVs, extracellular vesicles of H9C2 cells with stable overexpression of GDF-15; NC-EVs: extracellular vesicles of control H9C2 cells; MI, myocardial infarction; HF, heart failure; PCI, Percutaneous transluminal coronary intervention; mRNA, messenger ribonucleic acid; FBS, fetal bovine serum; NTA, nanoparticle tracking analysis; TEM, transmission electron microscopy; PBS, phosphate buffered saline; SDS, sodium dodecyl sulfate; CCK-8, Cell Counting Kit-8; PI, propidium iodide; RT-qPCR, quantitative real-time PCR; TSG101, tumor susceptibility gene 101 protein; CD63, lysosome-associated membrane protein 3; CD81, target of an antiproliferative antibody-1; BAX, BCL2L4; Bcl-2, B-cell lymphoma-2; P62, Sequestosome 1; Lc3, Map1LC3; TNF-α, tumor necrosis factor-α; IL-10, interleukin-10; IL-6, interleukin-6; β-actin, beta-actin; β-actin, beta-actin; GAPDH, Glyceraldehyde-3-phosphate dehydrogenase; TERT, telomerase reverse transcriptase; SD rats, Sprague Dawley rats; LVEF, left ventricular ejection fraction; LVFS, left ventricular fractional shortening; LVD, left ventricular diameter; LVAW, left ventricular anterior wall; LVPW, left ventricular posterior wall; LVW, left ventricular weight; NLRP3, NOD-like receptor thermal protein domain associated protein 3; HE, Haematoxylin-Eosin; CD31, platelet endothelial cell adhesion molecule-1; TUNEL, transferase dUTP nick end labelling; SEM, standard error of mean; ANOVA, one-way analysis of variance.

Data Sharing Statement

The datasets and materials used in the study are available from the corresponding author.

Ethics Approval and Consent to Participate

Animal experiments were conducted according to the Guidelines for the Care and Use of Laboratory Animals and were approved by the Ethics Committee of Nanjing Medical University (No. IACUC-2301020).

Author Contributions

All authors made a significant contribution to the work reported, whether that is in the conception, study design, execution, acquisition of data, analysis and interpretation, or in all these areas; took part in drafting, revising or critically

reviewing the article; gave final approval of the version to be published; have agreed on the journal to which the article has been submitted; and agree to be accountable for all aspects of the work.

Funding

Disclosure

The authors have declared that no competing interest exists in this work.

References

1. Zhao M, Nakada Y, Wei Y, et al. Cyclin D2 overexpression enhances the efficacy of human induced pluripotent stem cell-derived cardiomyocytes for myocardial repair in a swine model of myocardial infarction. *Circulation*. 2021;144(3):210–228. doi:10.1161/CIRCULATIONAHA.120.049497
2. Vogel B, Mehta SR, Mehran R. Reperfusion strategies in acute myocardial infarction and multivessel disease. *Nat Rev Cardiol*. 2017;14 (11):665–678. doi:10.1038/nrcardio.2017.88
3. Ong SB, Hernández-Reséndiz S, Crespo-Avilan GE, et al. Inflammation following acute myocardial infarction: multiple players, dynamic roles, and novel therapeutic opportunities. *Pharmacol Ther*. 2018;186:73–87. doi:10.1016/j.pharmthera.2018.01.001
4. Khan M, Nickoloff E, Abramova T, et al. Embryonic stem cell-derived exosomes promote endogenous repair mechanisms and enhance cardiac function following myocardial infarction. *Circ Res*. 2015;117(1):52–64. doi:10.1161/CIRCRESAHA.117.305990
5. Gallet R, Dawkins J, Valle J, et al. Exosomes secreted by cardiosphere-derived cells reduce scarring, attenuate adverse remodelling, and improve function in acute and chronic porcine myocardial infarction. *Eur Heart J*. 2017;38(3):201–211. doi:10.1093/eurheartj/ehw240
6. Rani S, Ryan AE, Griffin MD, Ritter T. Mesenchymal stem cell-derived extracellular vesicles: toward cell-free therapeutic applications. *Mol Ther*. 2015;23(5):812–823. doi:10.1038/mt.2015.44
7. Wang Y, Zhang L, Li Y, et al. Exosomes/microvesicles from induced pluripotent stem cells deliver cardioprotective miRNAs and prevent cardiomyocyte apoptosis in the ischemic myocardium. *Int J Cardiol*. 2015;192:61–69. doi:10.1016/j.ijcard.2015.05.020
8. Lou X, Zhao M, Fan C, et al. N-cadherin overexpression enhances the reparative potency of human-induced pluripotent stem cell-derived cardiac myocytes in infarcted mouse hearts. *Cardiovasc Res*. 2020;116(3):671–685. doi:10.1093/cvr/cvz179
9. Gao L, Gregorich ZR, Zhu W, et al. Large cardiac muscle patches engineered from human induced-pluripotent stem cell-derived cardiac cells improve recovery from myocardial infarction in swine. *Circulation*. 2018;137(16):1712–1730. doi:10.1161/CIRCULATIONAHA.117.030785
10. Yáñez-Mó M, Siljander PR, Andreu Z, et al. Biological properties of extracellular vesicles and their physiological functions. *J Extracell Vesicles*. 2015;4:27066. doi:10.3402/jev.v4.27066
11. Théry C, Witwer KW, Aikawa E, et al. Minimal information for studies of extracellular vesicles 2018 (MISEV2018): a position statement of the international society for extracellular vesicles and update of the MISEV2014 guidelines. *J Extracell Vesicles*. 2018;7(1):1535750. doi:10.1080/20013078.2018.1535750
12. Maas SLN, Breakefield XO, Weaver AM. Extracellular vesicles: unique intercellular delivery vehicles. *Trends Cell Biol*. 2017;27(3):172–188. doi:10.1016/j.tcb.2016.11.003
13. Sun L, Zhu W, Zhao P, et al. Long noncoding RNA UCA1 from hypoxia-conditioned hMSC-derived exosomes: a novel molecular target for cardioprotection through miR-873-5p/XIAP axis. *Cell Death Dis*. 2020;11(8):696. doi:10.1038/s41419-020-02783-5
14. Ibrahim AG, Cheng K, Marbán E. Exosomes as critical agents of cardiac regeneration triggered by cell therapy. *Stem Cell Reports*. 2014;2 (5):606–619. doi:10.1016/j.stemcr.2014.04.006
15. Zhang J, Lu Y, Mao Y, et al. IFN-γ enhances the efficacy of mesenchymal stromal cell-derived exosomes via miR-21 in myocardial infarction rats. *Stem Cell Res Ther*. 2022;13(1):333. doi:10.1186/s13287-022-02984-z
16. Kempf T, Eden M, Strelau J, et al. The transforming growth factor-beta superfamily member growth-differentiation factor-15 protects the heart from ischemia/reperfusion injury. *Circ Res*. 2006;98(3):351–360. doi:10.1161/01.RES.0000202805.73038.48
17. Xu J, Kimball TR, Lorenz JN, et al. GDF15/MIC-1 functions as a protective and antihypertrophic factor released from the myocardium in association with SMAD protein activation. *Circ Res*. 2006;98(3):342–350. doi:10.1161/01.RES.0000202804.84885.d0
18. Kempf T, Zarbock A, Widera C, et al. GDF-15 is an inhibitor of leukocyte integrin activation required for survival after myocardial infarction in mice. *Nat Med*. 2011;17(5):581–588. doi:10.1038/nm.2354
19. Wollert KC, Kempf T, Wallentin L. Growth differentiation factor 15 as a biomarker in cardiovascular disease. *Clin Chem*. 2017;63(1):140–151. doi:10.1373/clinchem.2016.255174
20. Wollert KC, Kempf T, Peter T, et al. Prognostic value of growth-differentiation factor-15 in patients with non-ST-elevation acute coronary syndrome. *Circulation*. 2007;115(8):962–971. doi:10.1161/CIRCULATIONAHA.106.650846
21. Kurrelmeyer KM, Michael LH, Baumgarten G, et al. Endogenous tumor necrosis factor protects the adult cardiac myocyte against ischemic-induced apoptosis in a murine model of acute myocardial infarction. *Proc Natl Acad Sci U S A*. 2000;97(10):5456–5461. doi:10.1073/pnas.070036297
22. Xiao T, Wei J, Cai D, et al. Extracellular vesicle mediated targeting delivery of growth differentiation factor-15 improves myocardial repair by reprogramming macrophages post myocardial injury. *Biomed Pharmacother*. 2024;172:116224. doi:10.1016/j.biopha.2024.116224

23. Wang Q, Zhang L, Sun Z, et al. HIF-1α overexpression in mesenchymal stem cell-derived exosome-encapsulated arginine-glycine-aspartate (RGD) hydrogels boost therapeutic efficacy of cardiac repair after myocardial infarction. *Mater Today Bio*. 2021;12:100171. doi:10.1016/j.mtbio.2021.100171

24. Sun L, Zhu W, Zhao P, et al. Down-regulated exosomal MicroRNA-221 - 3p derived from senescent mesenchymal stem cells impairs heart repair. *Front Cell Dev Biol*. 2020;8:263. doi:10.3389/fcell.2020.00263

25. Bär C, Bernardes de Jesus B, Serrano R, et al. Telomerase expression confers cardioprotection in the adult mouse heart after acute myocardial infarction. *Nat Commun*. 2014;5:5863. doi:10.1038/ncomms6863

26. Leri A, Franco S, Zacheo A, et al. Ablation of telomerase and telomere loss leads to cardiac dilatation and heart failure associated with p53 upregulation. *EMBO J*. 2003;22(1):131–139. doi:10.1093/emboj/cdg013

27. Oh H, Taffet GE, Youker KA, et al. Telomerase reverse transcriptase promotes cardiac muscle cell proliferation, hypertrophy, and survival. *Proc Natl Acad Sci U S A*. 2001;98(18):10308–10313. doi:10.1073/pnas.191169098

28. Herbert B, Pitts AE, Baker SI, et al. Inhibition of human telomerase in immortal human cells leads to progressive telomere shortening and cell death. *Proc Natl Acad Sci U S A*. 1999;96(25):14276–14281. doi:10.1073/pnas.96.25.14276

29. Li Q, Li N, Cui HH, et al. Tongxinluo exerts protective effects via anti-apoptotic and pro-autophagic mechanisms by activating AMPK pathway in infarcted rat hearts. *Exp Physiol*. 2017;102(4):422–435. doi:10.1113/EP086192

30. Liu L, Jin X, Hu CF, Li R, Zhou Z, Shen CX. Exosomes derived from mesenchymal stem cells rescue myocardial ischaemia/reperfusion injury by inducing cardiomyocyte autophagy via AMPK and Akt pathways. *Cell Physiol Biochem*. 2017;43(1):52–68. doi:10.1159/000480317

31. Qian L, Huang Y, Spencer CI, et al. In vivo reprogramming of murine cardiac fibroblasts into induced cardiomyocytes. *Nature*. 2012;485 (7400):593–598. doi:10.1038/nature11044

32. Suleiman M, Khatib R, Agmon Y, et al. Early inflammation and risk of long-term development of heart failure and mortality in survivors of acute myocardial infarction predictive role of C-reactive protein. *J Am Coll Cardiol*. 2006;47(5):962–968. doi:10.1016/j.jacc.2005.10.055

33. Huang P, Wang L, Li Q, et al. Combinatorial treatment of acute myocardial infarction using stem cells and their derived exosomes resulted in improved heart performance. *Stem Cell Res Ther*. 2019;10(1):300. doi:10.1186/s13287-019-1353-3

34. He JG, Li HR, Han JX, et al. GATA-4-expressing mouse bone marrow mesenchymal stem cells improve cardiac function after myocardial infarction via secreted exosomes. *Sci Rep*. 2018;8(1):9047. doi:10.1038/s41598-018-27435-9

35. Zheng YL, Wang WD, Cai PY, et al. Stem cell-derived exosomes in the treatment of acute myocardial infarction in preclinical animal models: a meta-analysis of randomized controlled trials. *Stem Cell Res Ther*. 2022;13(1):151. doi:10.1186/s13287-022-02833-z

36. Rackov G, Garcia-Romero N, Esteban-Rubio S, Carrión-Navarro J, Belda-Iniesta C, Ayuso-Sacido A. Vesicle-mediated control of cell function: the role of extracellular matrix and microenvironment. *Front Physiol*. 2018;9:651. doi:10.3389/fphys.2018.00651

37. Antimisiaris SG, Mourtas S, Marazioti A. Exosomes and exosome-inspired vesicles for targeted drug delivery. *Pharmaceutics*. 2018;10(4):218. doi:10.3390/pharmaceutics10040218

38. Singla DK. Stem cells and exosomes in cardiac repair. *Curr Opin Pharmacol*. 2016;27:19–23. doi:10.1016/j.coph.2016.01.003

39. Tan SJO, Floriano JF, Nicastro L, Emanueli C, Catapano F. Novel applications of mesenchymal stem cell-derived exosomes for myocardial infarction therapeutics. *Biomolecules*. 2020;10(5):707. doi:10.3390/biom10050707

40. Kalluri R, LeBleu VS. The biology, function, and biomedical applications of exosomes. *Science*. 2020;367(6478):eaau6977. doi:10.1126/science.aau6977

41. Figliolini F, Ranghino A, Grange C, et al. Extracellular vesicles from adipose stem cells prevent muscle damage and inflammation in a mouse model of hind limb ischemia: role of Neuregulin-1. *Arterioscler Thromb Vasc Biol*. 2020;40(1):239–254. doi:10.1161/ATVBAHA.119.313506

42. Bonaterra GA, Zügel S, Thogersen J, et al. Growth differentiation factor-15 deficiency inhibits atherosclerosis progression by regulating interleukin-6-dependent inflammatory response to vascular injury. *J Am Heart Assoc*. 2012;1(6):e002550. doi:10.1161/JAHA.112.002550

43. Lok SI, Winkens B, Goldschmeding R, et al. Circulating growth differentiation factor-15 correlates with myocardial fibrosis in patients with non-ischaemic dilated cardiomyopathy and decreases rapidly after left ventricular assist device support. *Eur J Heart Fail*. 2012;14(11):1249–1256. doi:10.1093/eurjhf/hfs120

44. Kempf T, Horn-Wichmann R, Brabant G, et al. Circulating concentrations of growth-differentiation factor 15 in apparently healthy elderly individuals and patients with chronic heart failure as assessed by a new immunoradiometric sandwich assay. *Clin Chem*. 2007;53(2):284–291. doi:10.1373/clinchem.2006.076828

45. Berezin AE, Berezin AA. Adverse cardiac remodelling after acute myocardial infarction: old and new biomarkers. *Dis Markers*. 2020;2020:1215802. doi:10.1155/2020/1215802

46. Bodnar AG, Ouellette M, Frolkis M, et al. Extension of life-span by introduction of telomerase into normal human cells. *Science*. 1998;279 (5349):349–352. doi:10.1126/science.279.5349.349

47. Blasco MA. Telomeres and human disease: ageing, cancer and beyond. *Nat Rev Genet*. 2005;6(8):611–622. doi:10.1038/nrg1656

48. Goytisolo FA, Samper E, Martín-Caballero J, et al. Short telomeres result in organismal hypersensitivity to ionizing radiation in mammals. *J Exp Med*. 2000;192(11):1625–1636. doi:10.1084/jem.192.11.1625

49. Minamino T, Miyauchi H, Yoshida T, Ishida Y, Yoshida H, Komuro I. Endothelial cell senescence in human atherosclerosis: role of telomere in endothelial dysfunction. *Circulation*. 2002;105(13):1541–1544. doi:10.1161/01.cir.0000013836.85741.17

50. Ogami M, Ikura Y, Ohsawa M, et al. Telomere shortening in human coronary artery diseases. *Arterioscler Thromb Vasc Biol*. 2004;24(3):546–550. doi:10.1161/01.ATV.0000117200.46938.e7

51. Santos JH, Meyer JN, Skorvaga M, Annab LA, Van Houten B. Mitochondrial hTERT exacerbates free-radical-mediated mtDNA damage. *Aging Cell*. 2004;3(6):399–411. doi:10.1111/j.1474-9728.2004.00124.x

52. Ale-Agha N, Jakobs P, Goy C, et al. Mitochondrial telomerase reverse transcriptase protects from myocardial ischemia/reperfusion injury by improving complex i composition and function. *Circulation*. 2021;144(23):1876–1890. doi:10.1161/CIRCULATIONAHA.120.051923

53. Ahmed S, Passos JF, Birket MJ, et al. Telomerase does not counteract telomere shortening but protects mitochondrial function under oxidative stress. *J Cell Sci*. 2008;121(Pt 7):1046–1053. doi:10.1242/jcs.019372

54. Zhu L, Zang J, Liu B, et al. Oxidative stress-induced RAC autophagy can improve the HUVEC functions by releasing exosomes. *J Cell Physiol*. 2020;235(10):7392–7409. doi:10.1002/jcp.29641

55. Beyer AM, Norwood Toro LE, Hughes WE, et al. Autophagy, TERT, and mitochondrial dysfunction in hyperoxia. *Am J Physiol Heart Circ Physiol*. 2021;321(5):H985–H1003. doi:10.1152/ajpheart.00166.2021

56. Moghadasi S, Elveny M, Rahman HS, et al. A paradigm shift in cell-free approach: the emerging role of MSCs-derived exosomes in regenerative medicine. *J Transl Med*. 2021;19(1):302. doi:10.1186/s12967-021-02980-6

57. Huang P, Wang L, Li Q, et al. Atorvastatin enhances the therapeutic efficacy of mesenchymal stem cells-derived exosomes in acute myocardial infarction via up-regulating long non-coding RNA H19. *Cardiovasc Res*. 2020;116(2):353–367. doi:10.1093/cvr/cvz139

58. Sun L, Ji Y, Chi B, et al. A 3D culture system improves the yield of MSCs-derived extracellular vesicles and enhances their therapeutic efficacy for heart repair. *Biomed Pharmacother*. 2023;161:114557. doi:10.1016/j.biopha.2023.114557

59. Chi B, Zou A, Mao L, et al. Empagliflozin-pretreated mesenchymal stem cell-derived small extracellular vesicles attenuated heart injury. *Oxid Med Cell Longev*. 2023;2023:7747727. doi:10.1155/2023/7747727

60. Chandy M, Rhee JW, Ozen MO, et al. Atlas of exosomal microRNAs secreted from human iPSC-derived cardiac cell types. *Circulation*. 2020;142 (18):1794–1796. doi:10.1161/CIRCULATIONAHA.120.048364

61. Gao L, Wang L, Wei Y, et al. Exosomes secreted by hiPSC-derived cardiac cells improve recovery from myocardial infarction in swine. *Sci Transl Med*. 2020;12(561):eaay1318. doi:10.1126/scitranslmed.aay1318